Electronic Supplementary Material (ESI) for Journal of Materials Chemistry C.


# Boron Subnaphthalocyanine Additive for Multilocus Passivation of Defects Towards Efficient and Stable Perovskite Solar Cells

*Qin Zhou[a,b,c], Chunsheng Cai[d], Qiu Xiong[a,b], Ping-Ping Sun[e], Zilong Zhang[a,b], Can Wang[a,b], Chi Li[a,b], Jingchuan Ye[c], Naoyuki Shibayama[f], Zhongyi Yuan[d], Peng Gao[a,b]**

[a.] *CAS Key Laboratory of Design and Assembly of Functional Nanostructures, and Fujian Provincial Key Laboratory of Nanomaterials Fujian Institute of Research on the Structure of Matter, Chinese Academy of Sciences, Fuzhou, Fujian 350002, China. E-mail: peng.gao@fjirsm.ac.cn*

[b.] *Laboratory for Advanced Functional Materials, Xiamen Institute of Rare Earth Materials, Haixi Institute, Chinese Academy of Sciences, Xiamen 361021, China*

[c.] *Institute of Carbon Neutrality and New Energy, School of Electronics and Information, Hangzhou Dianzi University, Hangzhou 310018, China*

[d.] *Institute of Polymers and Energy Chemistry (IPEC), College of Chemistry, Nanchang University, 999 Xuefu Avenue, Nanchang, 330031, China*

[e.] *Department of Chemistry, School of Science, Hainan University, Haikou 570228, China*

[f.] *Faculty of Biomedical Engineering Graduate School of Engineering Toin University of Yokohama 1614 Kurogane-cho, Aoba, Yokohama, Kanagawa 225–8503, Japan*

## Experimental Section

### 1. Materials

All the chemicals were used as received. All the ammonium salts were synthesized according to the previously reported methods[1], such as formamidinium iodide (FAI), methylammonium bromide (MABr), and methylammonium chloride (MACl). Lead iodide (99.99%) was purchased from TCI, while lead bromide (99.999%) was bought from Sigma-Aldrich. Bis(trifluoromethane) sulfonamide lithium salt (Li-TFSI), 4-tert-Butylpyridine (98%), N, N-dimethylformamide (DMF, 99.8%, anhydrous), dimethyl sulfoxide (DMSO, 99.9%, anhydrous), and chlorobenzene (CB, 99.8%, anhydrous) were purchased from Sigma-Aldrich. 2,2',7,7'-Tetrakis [N, N-di(4-methoxyphenyl) amino]-9,9'-spirobifluorene (Spiro-OMeTAD) was purchased from Shenzhen Feiming Science and Technology Co., Ltd. Synthesis of fluorinated subnaphthalocyanine triimides (B-SubPc-F) was referred to as previously reported methods. [2]

2. Device fabrication

Chemically etched fluorine-doped tin oxide (FTO) glass (7 Ω/sq, AGC glass) substrates were cleaned by ultrasonication in a detergent solution, rinsed thoroughly with deionized water, acetone, deionized water, and anhydrous ethanol, respectively, and then the substrates were dried with $N_2$ flow and further cleaned with plasma treatment for 5 min. Next, 100 uL of $SnO_2$ colloid solution (5 wt%, diluted from the commercially product of Alfa Aesar) was spin-coated onto the cleaned FTO substrates at 3000 rpm for 30 s, then annealed at 150 °C for 30 min in ambient air to form about 40 nm thickness $SnO_2$ electron transport layer (ETL). After that, the

$FA_{0.92}MA_{0.08}Pb(I_{0.92}Br_{0.08})_3$ perovskite precursor solution was prepared by dissolving 1.4 M FAI, 0.11 M MABr, 0.5 M MACl, 1.53 M $PbI_2$, and 0.11 M $PbBr_2$ in a mixed solvent of anhydrous DMF and DMSO in 8: 1, volume ratio. Then, the device fabrication, around 40 μL perovskite precursor solution, was spin-coated onto $SnO_2$ in a two-step procedure at 1000 rpm for 10 s with a ramp rate of 1000 rpm/s and 6000 rpm for 25 s with a ramp rate of 3000 rpm/s in a nitrogen glove box. After entering the second step, 150 μL of chlorobenzene (CB) was dropped on the spinning substrate in the last 5 s. For the B-SubPc-F containing samples (B-SubPc-F was dissolved in the CB antisolvent), the concentration of B-SubPc-F was tuned in the range of 0-0.06 mg/mL. To obtain uniform perovskite films, this was followed by annealing on a hotplate at 150 °C for 10 min. After the substrates were cooled to room temperature, 72.3 mg of Spiro-OMeTAD was dissolved in 1 mL of chlorobenzene with additives of 17.5 μL of Li-TFSI solution (520 mg/mL in acetonitrile), 28.8 μL of t-BP as hole transport material (HTM), which was spin-coated at 3000 rpm for 30 s with a ramp rate of 3000 rpm/s. Finally, 120 nm of the silver (Ag) counter electrode was deposited by thermally evaporated under a high vacuum.

3. Characterization

The top-view and cross-sectional view morphology of the perovskite films were observed using a field-emission scanning electron microscope (SEM, SUPRA 55, Zeiss, S2 Germany), operated at an acceleration voltage of 5 kV. The grazing incident wide-angle X-ray scattering (GIWAXS) measurements were performed at BL46XU beamline of SPring-8. The perovskite samples were prepared on the surface of FTO/$SnO_2$. The sample was irradiated with an X-ray energy of 12.39 keV ($\lambda$ = 1 Å) at

a fixed-incident angle on the order of 0.12° through a Huber diffractometer. The GIWAXS pattern was recorded with a two-dimensional image detector (Pilatus 300 K). XRD patterns of the films were obtained from an X-ray diffractometer (Rigaku Miniflex 600, Japan) with Cu Kα radiation. Fourier transform infrared (FTIR) spectrum analysis was performed using an FTIR spectrometer (Thermo Scientific Nicolet iS50) with an ATR accessory. UV-vis absorption spectra were recorded on a spectrophotometer (Agilent Cary 5000) in the 350-900 nm wavelength range at room temperature. The X-ray photoelectron spectrum (XPS) was performed using an X-ray photoelectron spectroscopy system (Axis Supra, Shimadzu). The steady-state PL spectra emissions were measured under 460 nm light source excitation using monochromatized Xe lamp, while the time-resolved PL decays (TRPL) were carried out with a picosecond pulsed diode laser excitation source (frequency 1 MHz and a fluence of ~ 1 nJ $cm^{-2}$) at a wavelength of 460 nm, using a fluorescence spectrophotometer (FLS980, Edinburgh Instruments). The current density-voltage (J–V) characteristics were measured using a solar simulator (3A class, Enli Tech) under AM 1.5G (100 mW $cm^{-2}$) illumination with calibrated light intensity by a KG-5 filter standard solar cell (SRC-2020), and the J–V data was recorded by a digital source meter (Keithley 2401) with 0.1V/s scan speed for both reverse and forward scan. During test, the 0.10 $cm^2$ area metal mask (Shenzhen Rigorous Technology Co. Ltd., calibrated in Shanghai Institute of Microsystem and Information Technology, CAS) was placed onto small area device. The External quantum effciency (EQE) was characterized by the QE-R systems (Enli Tech.), and the measurement scope was 300-900 nm. Electrical

impedance spectroscopy (EIS) measurement was carried out in the dark at 0.6 V applied voltages using an electrochemical workstation (Zennium Zahner, Germany) with an AC perturbation of 10 mV ranging from 0.1 Hz to 100 kHz, at room temperature with 40–50% humidity. The dark J–V characteristics of the devices were measured by a Keithley 2420 sourcemeter in the range of 0–3 V. Space-charge-limited current (SCLC) measurement based on the hole-only devices (ITO/PEDOT: PSS/perovskites (with/without B-SubPc-F)/Spiro-OMeTAD/Au) were fabricated to measure the hole trap density of the perovskites. The $N_{defects}$ is calculated by Equation S1[3].

$$N_{defects} = \frac{2V_{TFL}\varepsilon_r\varepsilon_0}{qL^2} \quad (S1)$$

where $V_{TFL}$ is onset voltage of the trap-filled limit region, $\varepsilon_r$ is the relative dielectric constant and $\varepsilon_0$ is the vacuum permittivity, q is the electronic charge, L is the perovskite films thickness.

Thermal admittance spectroscopy (TAS) test: The *tDOS* can be calculated by following differential function[4,5]:

$$N_T(E_\omega) = -\frac{V_{bi}\, dC\ \ \omega}{qWd\omega K_B T} \quad (S2)$$

and the corresponding energetic demarcation ($E_\omega$) can be defined with ω according to following function:

$$E_\omega = K_B T ln\left(\frac{\omega_0}{\omega}\right) \quad (S3)$$

Where $V_{bi}$, q, W, ω, $K_B$, T, $\omega_o$ presents the built-in potential, elementary charge, depletion width, angular frequency, Boltzmann constant, temperature, and the attempt-

to-escape frequency, respectively.

The $V_{bi}$ and W can be extracted from the Mott- Schottky plot. $V_{bi}$ was obtained from the following equation:

$$\frac{1}{C^2} = \frac{2(V_{bi} - V)}{A^2 e \varepsilon_0 \varepsilon N_d} \quad \text{(S4)}$$

The W was calculated using the following equation:

$$W = \sqrt{\frac{2\varepsilon_0 \varepsilon (V_{bi} - V)}{eN_d}} \quad \text{(S5)}$$

Where the $\varepsilon_0$, $\varepsilon$, A, $N_d$ presents vacuum dielectric constant, dielectric constant of perovskite materials, working area, and doping density, respectively.

4. Theoretical calculation:

The molecular geometries optimization and ESP were calculated using density functional theory (DFT) method at the B3LYP/6-31G(d,p) level of theory with the Gaussian 09 program package. Stationary points were verified by frequency analysis. The optimized structures were found to be stable. The calculated molecular electronic static potential (ESP) results were obtained with the Multiwfn 3.7 program.[6] For the mechanism of organic molecules doped in perovskite, the calculations were performed with DFT employing periodic boundary conditions using the Vienna ab initio simulation package (VASP).[7] The exchange correlation functional was described by Perdew-Burke-Ernzerhof (PBE) functional combining with the generalized gradient approximation (GGA). The ion-electron interactions were described by projected

augmented wave (PAW) method.[8] A plane wave basis set energy cut-off of 400 eV was employed in the calculation. The k-point meshes were sampled based on the Monkhorst-Pack method, a 4 × 4 ×1 k-point sampling was used for structural optimizations. All structures were allowed to relax during the optimization of the geometries with a conjugate gradient algorithm until the energy on the atoms is less than 1.0 × 10−5 eV, total energy calculations were achieved when the residual total energy of 0.01 eV and the maximal force of 0.01 eV/Å were reached. Van der Waals (vdW) correction was also considered by using Grimmer's DFT + D3 correction.[9] In our calculations, theoretical optimization was based on a penta-layered slab of FAPbI3 from the (001) surface using a 3 × 5 supercell, a 30 Å vacuum is added in the z direction. After geometry optimization, electron localization function (ELF) and bader charge were calculated with the k-point sampling of 8 × 8 ×1.

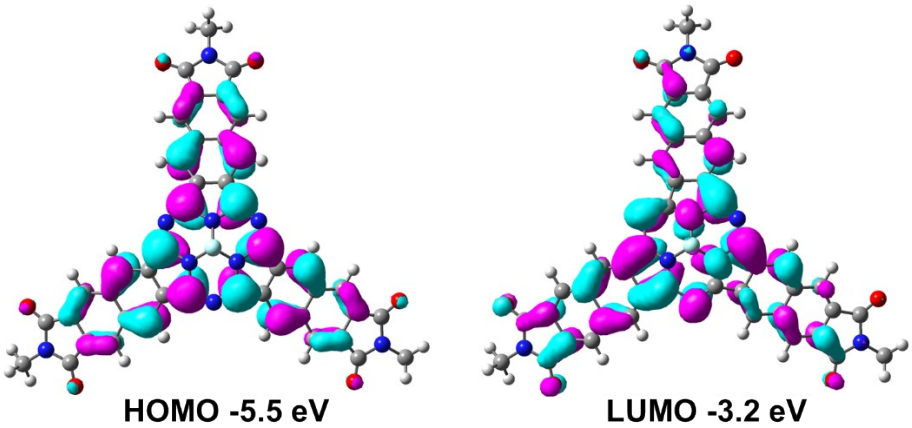


Figure S1. Optimized molecular configurations and corresponding LUMO and HOMO profiles for B-SubPc-F.

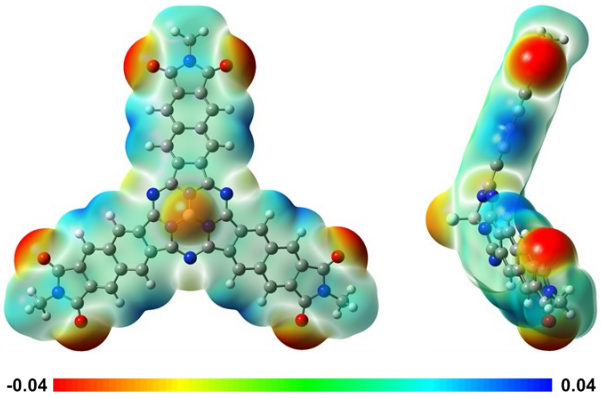


Figure S2. The surface electrostatic potential of B-SubPc-F.

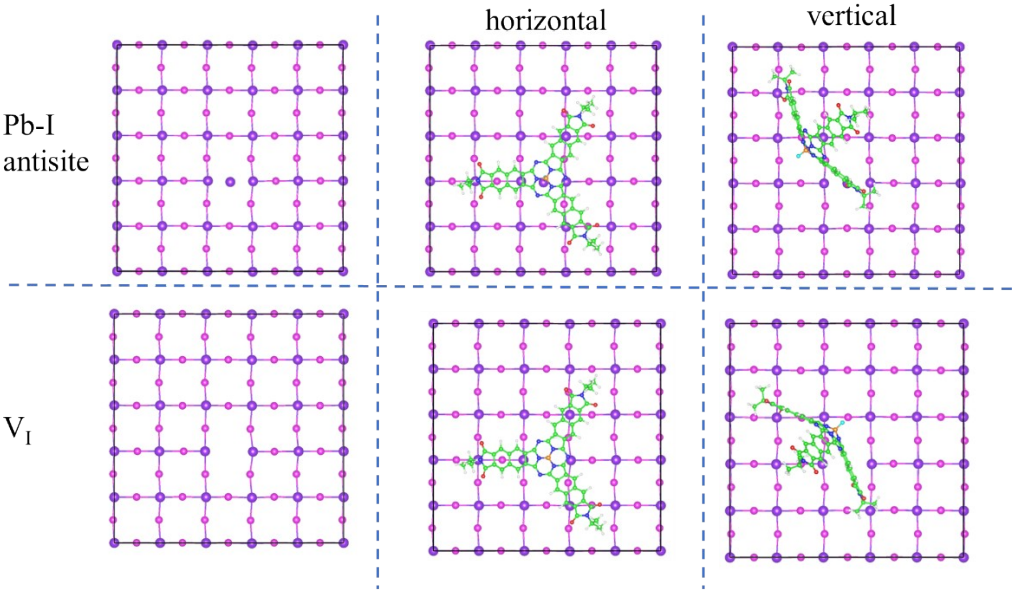


Figure S3. Schematic illustration of the $Pb_I$ anti-site defects and $V_I$, and the interaction between perovskite and B-SubPc-F for eliminating $Pb_I$ antisite defects and $V_I$ defects from top view (Pb: purple; I: magenta; C: green; N: blue; H: white; O: red; F: cyan; B: orange).

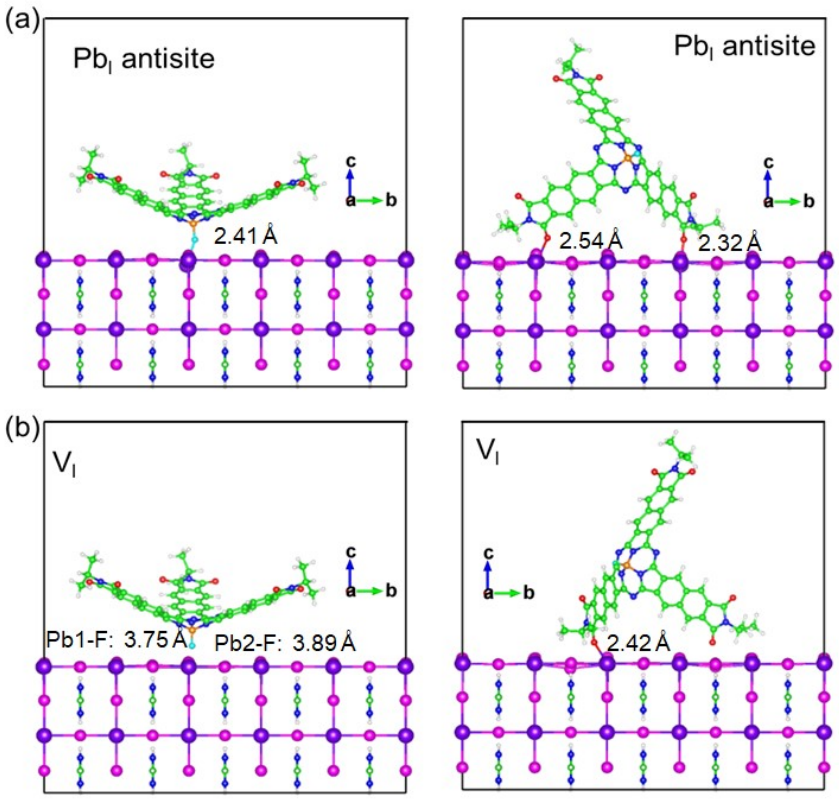


Figure S4. Schematic illustration of the interaction between perovskite and B-SubPc-F for eliminating a) $Pb_I$ antisite defects and b) $V_I$ defects from horizontal and vertical direction, respectively.

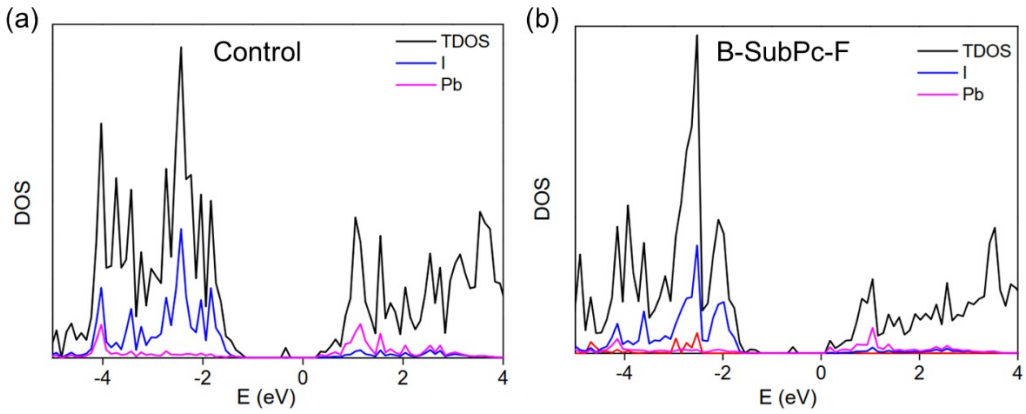


Figure S5. Calculated DOSs of (a) pure perovskite (110) surface with $Pb_I$ antisite defects and (b) perovskite with B-SubPc-F treatment.

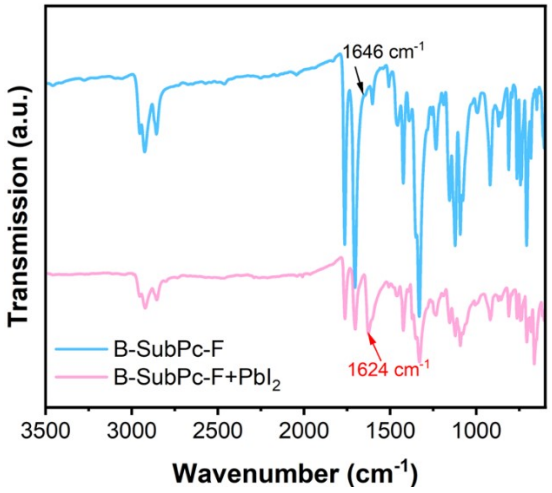


Figure S6. FTIR spectra of B-SubPc-F and B-SubPc-F-$PbI_2$ complex.

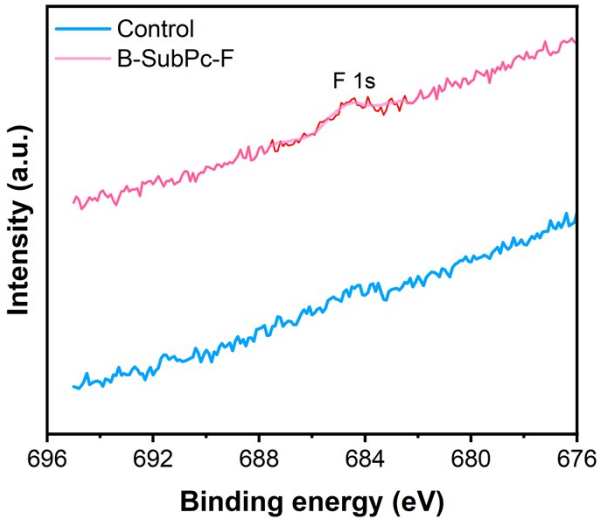


Figure S7. XPS spectra of F 1s for the perovskite films with and without B-SubPc-F treatment.

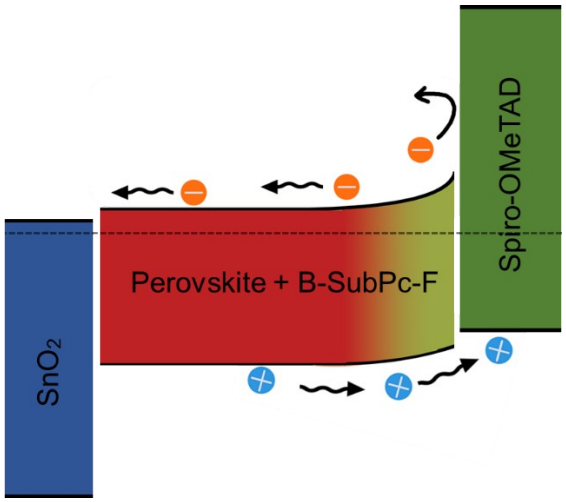


Figure S8. The band bending diagram at the perovskite surface.

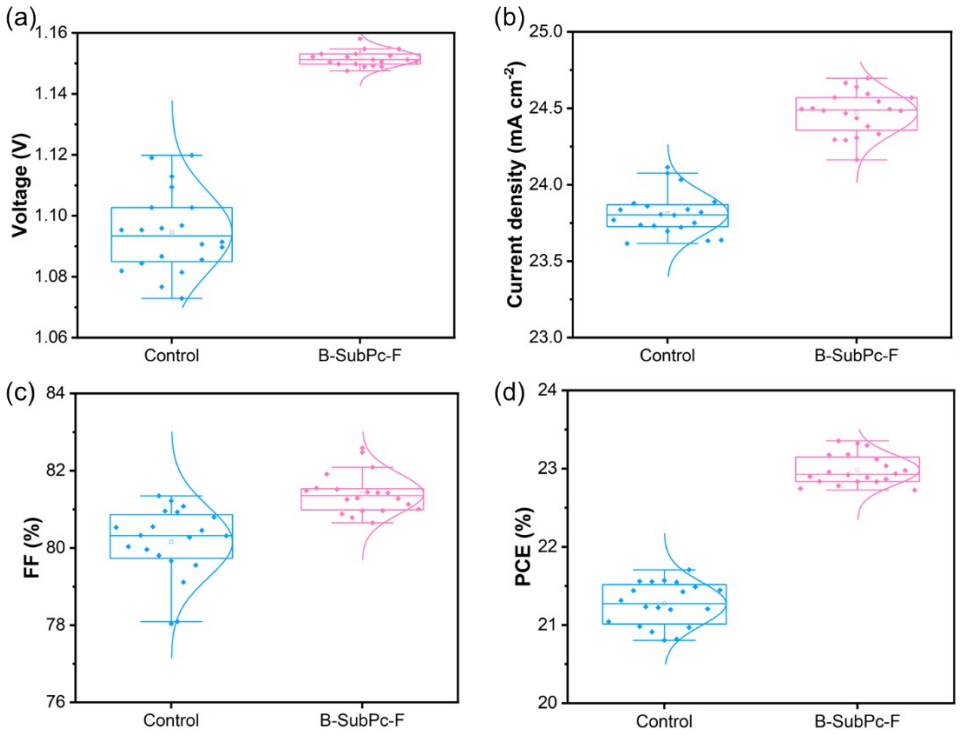


Figure S9. Performance distribution of the devices with and without B-SubPc-F treatment.

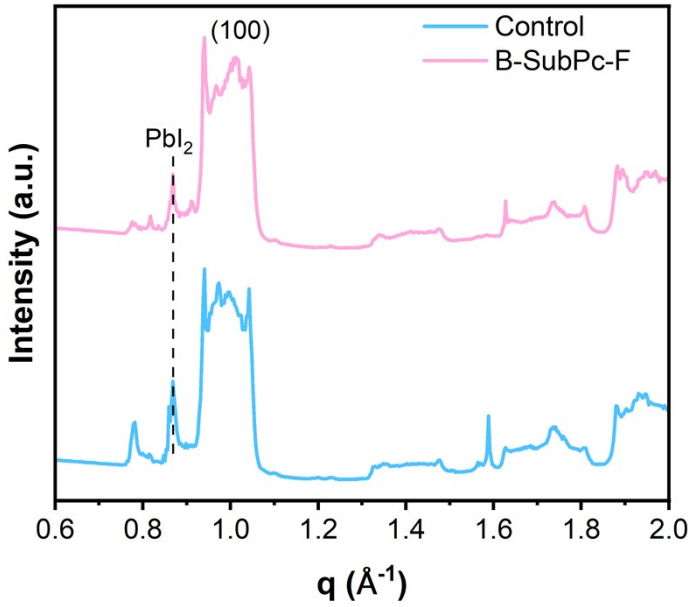


Figure S10. The 1D–GIWAXS data integral from corresponding 2D diffraction ring.

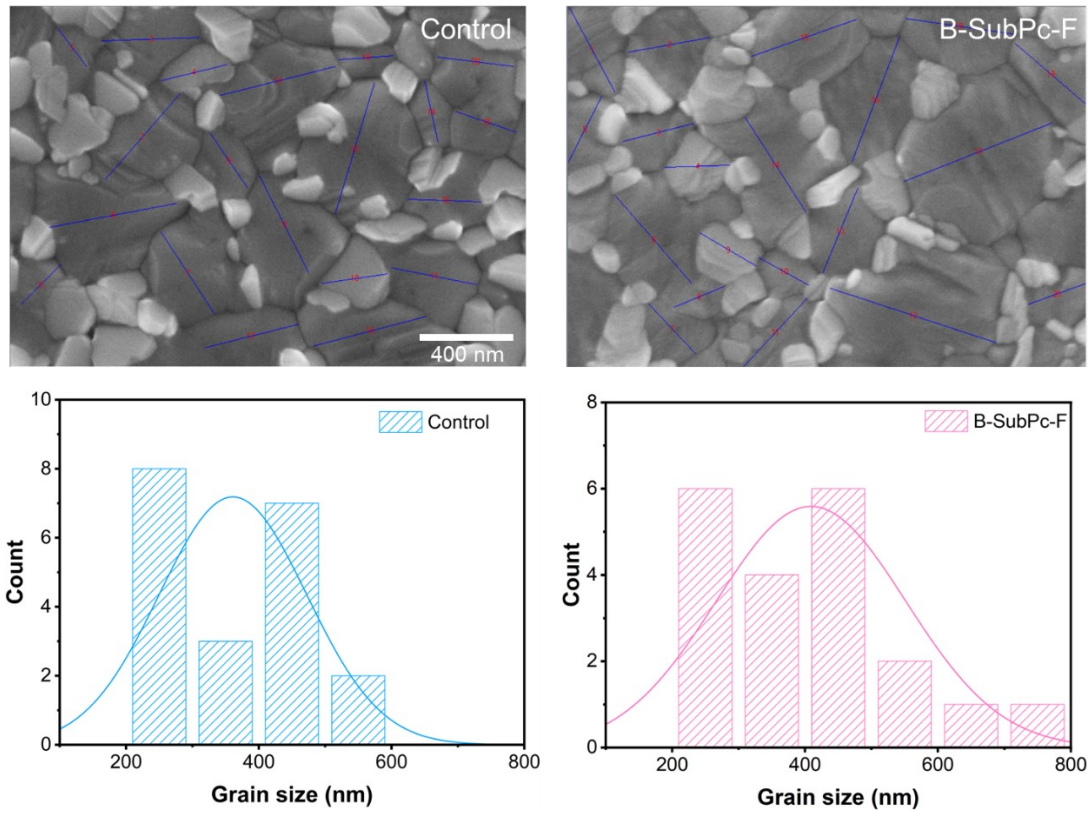


Figure S11. Grain size distributions of the control and B-SubPc-F-treated perovskite films.

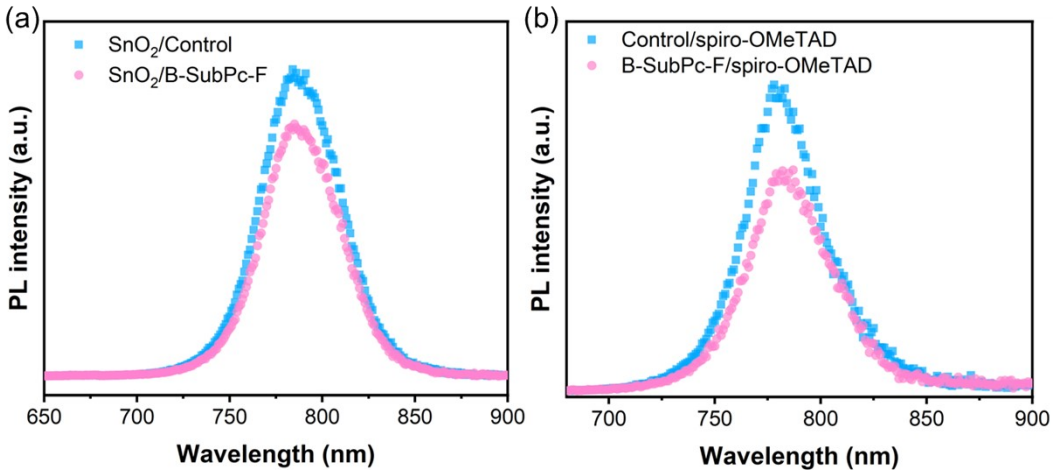


Figure S12. The PL spectra of perovskite films with/without B-SubPc-F a) $SnO_2$/perovskites and b) perovskites/spiro-OMeTAD.

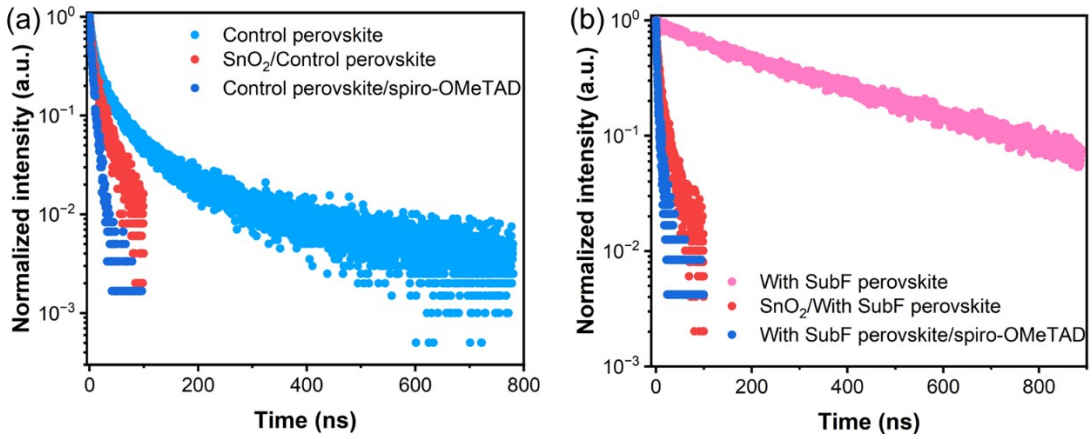


Figure S13. TRPL spectra of control (a) and B-SubPc-F-treated perovskite films (b) with $SnO_2$ and spiro-OMeTAD layer, respectively.

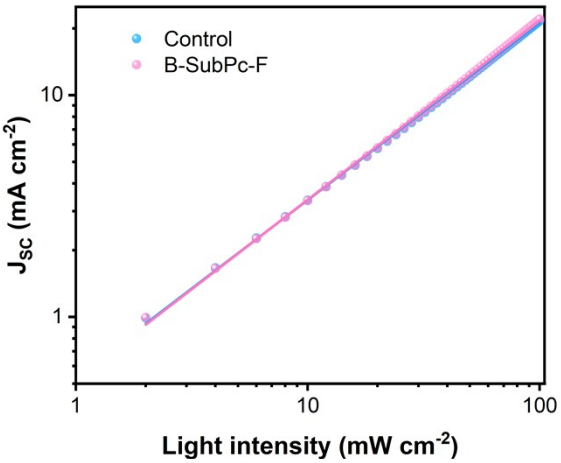


Figure S14. $J_{SC}$ vs. light intensity for the devices without and with B-SubPc-F treatment.

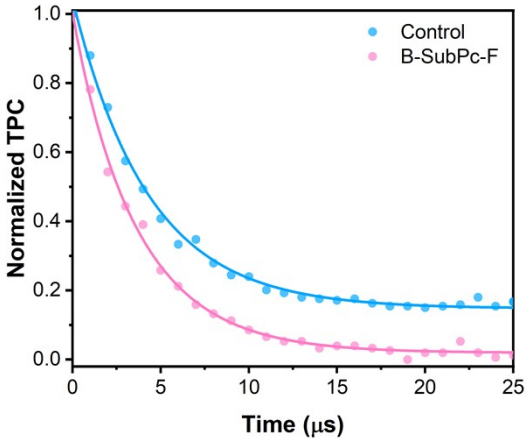


Figure S15. TPC for the devices without and with B-SubPc-F treatment.

Table S1. Coordinates of B-SubPc-F at B3LYP/6-31G(d,p) level of theory.

| Element | Coordinates (angstroms) |
|---|---|

| | X | Y | Z |
|---|---|---|---|
| N | 1.34655800 | -0.23880900 | 2.12202800 |
| C | 2.15760400 | 0.78387700 | 1.70819200 |
| N | 1.71945900 | 2.04441300 | 1.57537300 |
| C | 0.40252600 | 2.25978800 | 1.70826400 |
| N | -0.46591300 | 1.28548300 | 2.12249200 |
| B | 0.00023800 | -0.00025700 | 2.74020600 |
| C | -0.43866800 | 3.33220200 | 1.18902300 |
| C | -1.79900500 | 2.83861200 | 1.18901200 |
| C | -1.75693600 | 1.47627100 | 1.70800300 |
| C | 1.75625100 | -1.47803400 | 1.70800900 |
| C | 3.10563900 | -1.28575600 | 1.18914700 |
| C | 3.35851500 | 0.13912300 | 1.18922600 |
| N | 0.91128900 | -2.51092300 | 1.57485500 |
| N | -2.62957500 | 0.46669800 | 1.57488600 |
| N | -0.87952300 | -1.04623600 | 2.12093700 |
| C | -2.15757900 | -0.78148000 | 1.70731200 |
| C | -2.66593600 | -2.04625000 | 1.18863600 |
| C | -1.55835800 | -2.97764500 | 1.18834000 |
| C | -0.39947600 | -2.25998100 | 1.70715000 |
| C | -0.14055000 | 4.57973800 | 0.68167800 |
| C | -1.18420300 | 5.39393100 | 0.18205300 |
| C | -2.54900400 | 4.89872200 | 0.18223900 |
| C | -2.82777300 | 3.60477800 | 0.68199500 |
| C | -0.90982300 | 6.69962100 | -0.32875000 |
| C | -1.94807100 | 7.44976000 | -0.80478600 |
| C | -3.28124000 | 6.96594900 | -0.80476200 |
| C | -3.59689900 | 5.72462600 | -0.32845200 |
| C | 4.03674700 | -2.16778700 | 0.68160100 |

| | | | |
|---|---|---|---|
| C | 5.26336200 | -1.67113100 | 0.18125900 |
| C | 5.51705200 | -0.24158500 | 0.18108000 |
| C | 4.53617400 | 0.64687500 | 0.68137900 |
| C | 6.25664900 | -2.56177700 | -0.32970600 |
| C | 7.42425600 | -2.03768900 | -0.80847800 |
| C | 7.67212000 | -0.64128500 | -0.80866600 |
| C | 6.75610600 | 0.25274700 | -0.33015400 |
| C | -3.89551300 | -2.41159700 | 0.68166600 |
| C | -4.07902400 | -3.72236400 | 0.18164900 |
| C | -2.96792700 | -4.65688500 | 0.18127600 |
| C | -1.70775500 | -4.25159100 | 0.68086000 |
| C | -5.34706100 | -4.13708600 | -0.32924900 |
| C | -5.47796600 | -5.41125000 | -0.80543200 |
| C | -4.39272600 | -6.32427700 | -0.80547300 |
| C | -3.15964500 | -5.97727800 | -0.32959400 |
| C | -6.66323800 | -6.10215600 | -1.38895700 |
| N | -6.22234200 | -7.39759200 | -1.70758900 |
| C | -4.87073500 | -7.61038900 | -1.38861500 |
| C | -1.95418800 | 8.82151400 | -1.38868400 |
| N | -3.29638300 | 9.08643000 | -1.70853900 |
| C | -4.15624700 | 8.02223500 | -1.38901200 |
| C | 8.61581900 | -2.71878300 | -1.39062000 |
| N | 9.51751600 | -1.68926100 | -1.70852800 |
| C | 9.02540000 | -0.41219800 | -1.39077300 |
| O | -7.78629800 | -5.67723600 | -1.57430700 |
| O | -4.26007900 | -8.64433200 | -1.57354500 |
| O | -5.35694200 | 8.00975100 | -1.57446200 |
| O | -1.02499100 | 9.58217400 | -1.57354600 |
| O | 9.61912800 | 0.63302600 | -1.56750200 |

| | | | |
|---|---|---|---|
| O | 8.81317800 | -3.90455400 | -1.56737300 |
| C | -7.07546000 | -8.41154300 | -2.30109400 |
| C | 10.81980000 | -1.92042200 | -2.30753000 |
| C | -3.74836900 | 10.33153100 | -2.30318000 |
| F | -0.00010300 | -0.00127400 | 4.12184000 |
| H | 0.88321800 | 4.94201300 | 0.66570100 |
| H | -3.84568000 | 3.22639100 | 0.66618300 |
| H | 0.10748500 | 7.08094100 | -0.33503200 |
| H | -4.62205700 | 5.36493100 | -0.33449900 |
| H | 3.83852600 | -3.23553000 | 0.66571100 |
| H | 4.71754000 | 1.71759900 | 0.66539600 |
| H | 6.07892400 | -3.63357400 | -0.33392300 |
| H | 6.95816200 | 1.32024000 | -0.33458700 |
| H | -4.72104300 | -1.70599600 | 0.66610600 |
| H | -0.87126000 | -4.94412700 | 0.66467400 |
| H | -6.18577100 | -3.44650400 | -0.33522200 |
| H | -2.33573900 | -6.68547500 | -0.33598800 |
| H | -7.57390600 | -9.00724500 | -1.52850400 |
| H | -7.83287000 | -7.91529300 | -2.91048100 |
| H | -6.45798300 | -9.07050000 | -2.91412900 |
| H | 10.75869600 | -1.90096700 | -3.40119600 |
| H | 11.50002800 | -1.13373900 | -1.97619700 |
| H | 11.17926200 | -2.90059300 | -1.98927400 |
| H | -2.93990400 | 10.73931400 | -2.91259300 |
| H | -4.62739400 | 10.12517700 | -2.91639600 |
| H | -4.01592200 | 11.06153800 | -1.53135800 |

Energy= -2796.583053 (Hartree); Dipole Moment=0.089969 (Debye); |Isovalue| for new surfaces: MO= 0.0200, Density= 0.0004.

Table S2. Photovoltaic performance values in reverse scan direction of the control and B-SubPc-F-incorporated devices with concentration optimization.

| Samples | $V_{OC}$ (V) | $J_{SC}$ (mA $cm^{-2}$) | FF (%) | PCE (%) |
|---|---|---|---|---|
| Control | 1.119 | 23.90 | 81.33 | 21.75 |
| 0.02 mg $mL^{-1}$ | 1.135 | 23.81 | 84.39 | 22.81 |
| 0.04 mg $mL^{-1}$ | 1.152 | 24.85 | 81.54 | 23.35 |
| 0.06 mg $mL^{-1}$ | 1.142 | 23.74 | 82.53 | 22.38 |

Table S3. Average values of $V_{OC}$, $J_{SC}$, FF, and PCE of more than 20 devices in RS directions.

| Samples | $V_{OC}$ (V) | $J_{SC}$ (mA $cm^{-2}$) | FF (%) | PCE (%) |
|---|---|---|---|---|
| Control | 1.095±0.013 | 23.81±0.138 | 80.15±0.921 | 21.27±0.275 |
| B-SubPc-F | 1.152±0.003 | 24.47±0.140 | 81.41±0.524 | 22.98±0.194 |

Table S4. Fitting parameters for time-resolved PL decay from control and B-SubPc-F-incorporated perovskite films.

| Samples | $\tau_1$(ns) | $\tau_2$(ns) | $A_1$ | $A_2$ | $\tau_{ave}$ (ns) |
|---|---|---|---|---|---|
| Control | 20.76 | 108.04 | 0.88 | 0.12 | 56.99 |
| $SnO_2$/Control | 3.56 | 19.03 | 0.65 | 0.39 | 15.41 |
| Control/spiro-OMeTAD | 2.61 | 7.83 | 0.56 | 0.48 | 6.37 |
| B-SubPc-F | 55.58 | 341.28 | 0.15 | 0.85 | 333.30 |
| $SnO_2$/B-SubPc-F | 3.34 | 17.03 | 0.67 | 0.38 | 13.51 |
| B-SubPc-F/spiro-OMeTAD | 2.23 | 9.37 | 0.77 | 0.22 | 6.13 |

Table S5. EIS derived series resistance (Rs), the contact resistance ($R_{co}$) and recombination resistance (Rrec) for the different devices.

| Samples | $R_s$ (Ω) | $R_{co}$ (kΩ) | $R_{rec}$ (kΩ) |
|---|---|---|---|
| Control | 17.55 | 11.6 | 84 |
| B-SubPc-F | 15.06 | 7.14 | 97 |

References


1 Q. Zhou, L. Liang, J. Hu, B. Cao, L. Yang, T. Wu, X. Li, B. Zhang and P. Gao, *Adv. Energy Mater.*, 2019, **9**, 1802595.

2 C. Cai, S. Chen, L. Li, Z. Yuan, X. Zhao, Y. Zhang, Y. Hu, C. Yang, M. Hu, X. Huang, X. Chen and Y. Chen, *J. Mater. Chem. C*, 2020, **8**, 2186–2195.

3 D. Ma, A. I. Hümmelgen, B. Hu and F. E. Karasz, *J. Phys. D. Appl. Phys.*, 1999, **32**, 2568–2572.

4 J.-W. Lee, D.-H. Kim, H.-S. Kim, S.-W. Seo, S. M. Cho and N.-G. Park, *Adv. Energy Mater.*, 2015, **5**, 1501310.

5 S. Khelifi, K. Decock, J. Lauwaert, H. Vrielinck, D. Spoltore, F. Piersimoni, J. Manca, A. Belghachi and M. Burgelman, *J. Appl. Phys.*, 2011, **110**, 094509.

6 T. Lu and F. Chen, *J. Comput. Chem.*, 2012, **33**, 580–592.

7 J. P. Perdew, K. Burke and M. Ernzerhof, *Phys. Rev. Lett.*, 1996, **77**, 3865–3868.

8 D. Joubert, *Phys. Rev. B - Condens. Matter Mater. Phys.*, 1999, **59**, 1758–1775.

9 S. Grimme, J. Antony, S. Ehrlich and H. Krieg, *J. Chem. Phys.*, 2010, **132**, 154104.